We are IntechOpen, the world's leading publisher of Open Access books Built by scientists, for scientists

4,800
Open access books available

122,000
International authors and editors

135M
Downloads

Our authors are among the

154
Countries delivered to

TOP 1%
most cited scientists

12.2%
Contributors from top 500 universities

CLARIVATE ANALYTICS BOOK CITATION INDEX INDEXED

WEB OF SCIENCE™

Selection of our books indexed in the Book Citation Index in Web of Science™ Core Collection (BKCI)

Interested in publishing with us?
Contact book.department@intechopen.com

Numbers displayed above are based on latest data collected.
For more information visit www.intechopen.com

18

Design of dielectric lens antennas by multi-objective optimization

Yoshihiko Kuwahara † and Takashi Maruyama ‡
† *Shizuoka University,* ‡ *NTT*
Japan

1. Introduction

Lens antennas are a promising device for realizing the anti-collision radars needed in intelligent transport systems (ITS) and multibeam antennas for satellite communication. They have simple structure, high gain and no feed blockage. Especially if the operating frequencies are above the microwave band, the resulting apertures with several tens of wavelengths, become practical.

In advance ITS application, the antenna is expected to resolve several objects in azimuth plane. In satellite application, the terrestrial station should catch multiple satellites at various directions. These applications demand multibeam antennas.

Typical antennas with multibeam attributes include the dual-reflector bifocal antenna (Rao, 1974). Another proposal is the bifocal lens (Brown, 1956), its multibeam characteristics has been evaluated (Peebles, 1988). Multibeam antennas have to form high gain and low sidelobe radiation patterns at different directions. The bifocal lens is guaranteed to equalize the aperture phase distribution on the specified design directions in the scanning plane. However, it is not guaranteed on the transverse plane due to its astigmatism, and no previous report has adequately addressed the design issues, especially the resulting degradation of the radiation pattern. Another multibeam lens antenna is the Luneburg lens (Luneburg, 1964). Though it offers many focal points at arbitrary directions, it has manufacturing problems, tapered dielectric constant, and heavy weight.

Our solution is to propose an effective method that optimizes multibeam lens antennas by gain, beamwidth, and sidelobe level. Antenna designs based on GA are very attractive and various methods have been proposed (Altshuler & Linden, 1997; Jones & Joines, 1997); we have already proposed a Yagi-Uda antenna design based on the pareto-GA (Kuwahara, 2005).

This chapter presents the design of a multibeam lens antenna based on the pareto-GA. The coordinates of the lens shape and the feed position are given as variables and are associated with GA chromosomes. From the variables, the radiation patterns are calculated. The values of the objective functions are evaluated from the radiation pattern. The objective functions are given as the gain and the sidelobe level on the scanning plane and the transverse plane.

To balance these objective functions, we adopt the pareto-GA (Fonseca & Fleming, 1993). In the pareto-GA, individuals are ranked through multiple objective functions and selection

and crossover are carried out. To obtain rapid convergence, elitist preserving selection (Jong, 1975) is applied. As a result, various lenses that offer well balanced performance including the gain-tuned lens and the sidelobe level-tuned lens are obtained.
For the collision avoidance radar in the short range, it is necessary to search targets over wide angle in the azimuth plane. In addition, considering the road inclination, the beamwidth in the elevation plane should be wide enough so as not to miss any of the targets. That is, the antenna should form multibeams with the fan beam in the elevation plane. To achieve such characteristics, we introduce the elliptical aperture. We demonstrate the proposed method can balances three objects; the desired beam width in the elevation plane in addition to multibeams with high gain and low sidelobe levels.

2. Multi-objective Optimization by the Genetic Algorithm

2.1 Overview

The Genetic algorithm (GA) is one of the techniques used for solving the optimization problem under specified constraint conditions. The antenna is designed to obtain structural parameters that satisfy the requirements of various performances such as gain, beam width, largest side lobe level, and input impedance. In the case of an optimization method such as the steepest gradient method, it is difficult to apply a suitable initial parameter because structural parameters have complex influences on antenna performances. The GA is very attractive because it can globally obtain optimal solutions (Haupt & Haupt, 1998; Rahmat-Samii & Michielessen, 1999; Werner & Mittra, 2000; Alshuler & Linden, 1997; Jones & Joines, 1997).
Using the GA, the structural parameters of the Yagi-Uda antenna were optimized. And the gain, backlobe, and input impedance obtained by the GA and the values obtained by the steepest gradient method were compared (Jones & Joines, 1997). They have reported that the design parameters obtained by the GA yield better performances than those obtained by the gradient method. In their paper, the objective function of the GA is expressed by weighting the sum of a large number of objective functions to optimize multiple performances. In other words, the multi-objective optimization problem was transformed into a simple optimization problem with a single objective function. Although the weight determination method was not mentioned in their paper, it can be considered that they have repeatedly conducted computer experiments using empirical values.
The Pareto GA addresses a multi-objective optimization problem with a Pareto-optimal set (non-dominated solutions) in a very efficient manner (Fonseca & Fleming, 1993) since it can obtain a Pareto-optimal set in a single trial of a numerical simulation. Recently, the Pareto GA has been applied to the electromagnetic field and antenna design. The multi-layer microwave absorbers were optimized and the trade-off between reflectivity and thickness were studied (Weile et al., 1996; Weile & Michielssen, 1997). Further, they applied the Pareto GA to the array antenna with digital phase shifters for a low beamwidth and side lobe level (Weile & Michielssen, 1996). Furthermore, the feed circuits of a wing mounted Log-Periodic monopole array were optimized (Fisher et al., 1999). In their paper, the trade-off among the field degradation, feed reflection, and feed inefficiency over the operating band has been investigated. Electrically small planar antennas with an inductively coupled feed structure were designed (Choo & Ling, 2003). In this case, the trade-off between the efficiency-bandwidth product and the antenna size has been discussed.

We have also introduced the Pareto GA into the Yagi-Uda antenna design. In order to ensure diversity in Pareto-optimal solutions, individual fitness values selected by the Pareto ranking (Fonseca & Fleming, 1993) were corrected using fitness sharing (Horn et al., 1994). In addition, the elitist preserving selection process (Jong, 1975) was applied to accelerate convergence. We have demonstrated that the Pareto GA was able to search various Pareto-optimal solutions in a single trial of the GA process including the relatively small number of generations, and that it was a design method that was able to solve a multi-objective optimization problem such as the Yagi-Uda antenna design in a highly efficient manner.

2.2 Various multi-objective optimization

(1) Transforming a Multiobjective Optimization Problem into a Single Objective Optimization Program.

In order to apply the conventional GA to a multi-objective optimization problem, this method weighs multi-objective functions and combines them linearly to form a single-objective function that is to be solved. Assuming that the parameter vector x represents the structure of an antenna, the antenna is designed to determine the x that minimizes the side lobe level SLL(x), maximizes the gain G(x), and achieves an input impedance Z(x) of approximately 50 Ω. Thus, the objective function y expressed by Equ. (1) is maximized to solve a single-objective optimization problem.

$$y = aG - b\left|50 - \mathrm{Re}(Z(x))\right| - c\left|\mathrm{Im}(Z(x)\right| - dSLL(x) \tag{1}$$

where a, b, c, and d are positive weight constants. The only guiding principles for determining their values are to increase a when priority is given to the gain, to increase b and c when priority is given to the impedance matching, and to increase d when priority is given to the side lobe level. In order to obtain Pareto-optimal solutions, the GA process should be attempted for several combinations of weight constants (a, b, c, and d). The process of determining the weight constants has not been mentioned in literature (Alshuler & Linden, 1997; Jones & Joines, 1997). Accordingly, previous studies might have determined the weight constants by numerical experiments, resulting in a less efficient calculation.

(2) VEGA (Scaffer, 1985)

The algorithm of VEGA (Vector Evaluated GA) begins with the selection of individuals that are to be left behind for the next generation, with every objective function to form a new population. It then carries out crossover and mutation processes following the random selection of individuals on the basis of the size of the original population from which the new population is generated. Although VEGA does not require uniquely undeterminable weight constants, such as a, b, c, and d, which are used in Equ. (1), it has difficulties in obtaining various Pareto-optimal solutions. These difficulties are due to the fact that the Pareto-optimal solutions obtained by VEGA have a tendency of lying very close to each other in solution space.

(3) Pareto GA

In order to efficiently obtain various Pareto-optimal solutions in a single trial of the GA process, we apply the Pareto GA. Further, the elitist preserving selection process is applied for rapid convergence.

1)Pareto GA

The VEGA is a non-Pareto approach that selects every objective function of the individuals. On the other hand, Pareto ranking is a Pareto approach that selects on the basis of the merits and demerits of the solutions from among the Pareto-optimal solutions.

The Pareto ranking procedure for optimizing two objective functions is shown in Fig. 1. The horizontal and vertical axes of Fig. 1 indicate the values of the objective functions 1 and 2, respectively. The further the point of the objective function is from the origin, the larger is its value. The white circle represents the set of values of the objective functions 1 and 2, which is a function of each individual xi. The ranking of the Pareto-optimal solution in the group is assigned as 1. As regards the individuals that are not Pareto-optimal solutions, the ranking is lowered by the number of individuals that are dominated by others. The individual denoted by 1 in Fig. 1 is a Pareto-optimal solution. The ranking of individual E is 2 because it is dominated by individual B. The ranking of G is also 2 because it is dominated by individual C in a similar manner. The ranking of F is 3 because it is dominated by individuals B and C. The ranking of individual H is 5 because it is dominated by individuals B, C, E, and F. When the Pareto ranking is applied, the fitness $f(x_i)$ of an individual x_i is expressed by Equ. 2.

$$f(x_i) = \frac{1}{N_i}, \tag{2}$$

where Ni is the ranking of an individual xi, which is obtained by the Pareto ranking.

2)Elitist preserving selection

The following methods are examples of individual selection schemes after crossover.

(1)SGA (Simple GA), by which children are unconditionally chosen after crossover.

(2)ER (Elitist Recombination), by which two individuals whose fitness is higher than the others are chosen from among four individuals, two parents and two children.

(3)Elitist preserving selection, by which individuals are chosen on the basis of the original population size in a descending order of fitness from among all the individuals of two generations, before and after the crossover.

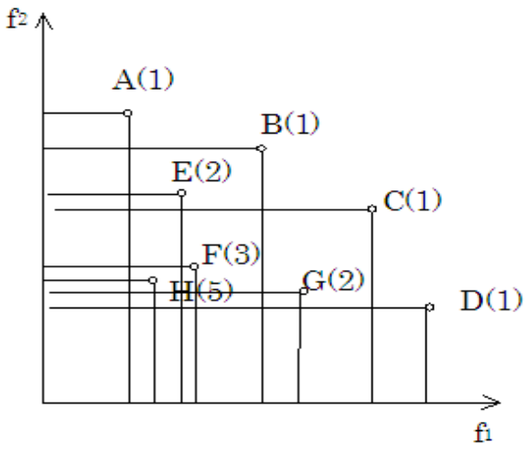

Fig. 1. Pareto Ranking

The elitist preserving selection scheme accelerates convergence because the population after the crossover consists of individuals with higher fitness. According to our numerical experiments, elitist preserving selection causes acceleration in the convergence speed that is several times higher than the SGA.

3. Design of dielectric lens antennas by Pareto Genetic Algorithm

3.1 Radiation Pattern of the Lens Antenna

(1) Basic Theory

To calculate the radiation pattern of a lens antenna, it is necessary to obtain the amplitude distribution and the phase distribution on the aperture. These are calculated by means of ray tracing (Tajima, 2004). The ray tracing model is shown in Fig. 2. Here the inner side of the lens is defined as the first plane and outer side is defined as the second plane. The feed is placed away from the center axis of the lens. In this situation, the whole lens plane is swept by ray tracing to obtain the amplitude and the phase distribution as $E(x,y)$ and $\Theta(x,y)$, respectively. $\Theta(x,y)$ is given by,

$$\Theta(x,y) = - k\, l_e(x,y) \tag{3}$$

$$l_e(x,y) = l_1(x,y) + ref\, l_2(x,y) + l_3(x,y), \tag{4}$$

where, k is the wavenumber, $l_e(x,y)$ is the path length from the feed to the aperture plane, and ref is the refractive index of the lens. From the power conservation law, the power incident to the first plane is preserved at the aperture plane. The calculation involves multiplying the power density by its associated area. Thus $E(x,y)$ can be calculated from the next relation (Lee, 1988).

$$D_0(\theta_0)\, dS = E(x,y)^2 dS' \tag{5}$$

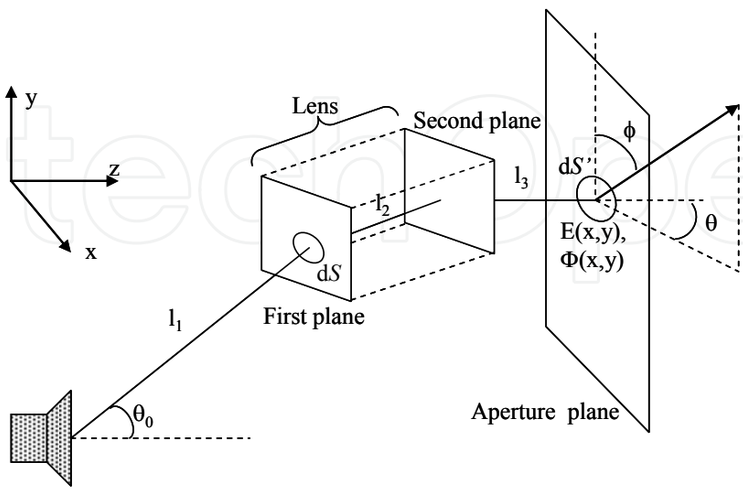

Fig. 2. Ray tracing model

The left term represents the incident power to the lens. $D_0(\theta_0)$ is the feed power pattern, and θ_0 is the angle from the direction of the normal to the feed aperture. dS is a small area that is perpendicular to the ray. dS' is the projection of dS on the aperture plane. The radiation pattern, $E_r(\theta, \phi)$, is calculated by the next formula.

$$E_r(\theta,\phi) = \iint E(x,y)\exp(\, j\Theta(x,y) + jk(x\sin(\theta) + y\cos(\phi))\,)\,\mathrm{d}y\mathrm{d}x \tag{6}$$

ϕ is the angle from the x-axis on the xy-plane and θ is the angle from the z-axis on the plane including ϕ.

(2) Single Focal Lens

We describe an analysis for a single focal lens. The coordinate system is shown in Fig.3. $P_1(n)$ and $P_2(n)$ denote coordinates of first and second plane in the cross section including the lens' center axis. Rotating symmetry around the center axis is assumed for the lens. When ray tracing from Feed(1) to the reference plane for each path is carried out, all phase should be arranged on the reference plane. The reference plane is set above second plane. All coordinates are decided so as to satisfy with Equ. (7).

$$l_e(n)=\text{const} \quad (n=1\cdots N) \tag{7}$$

Fig.4 shows a ray tracing example for the plano-convex lens. The second plane coordinates are decided so as to satisfy Equ. (7) and Snell's law. At z=25 (the reference plane), all path lengths are the same and all paths are parallel. The radiation pattern is also shown Fig.5.

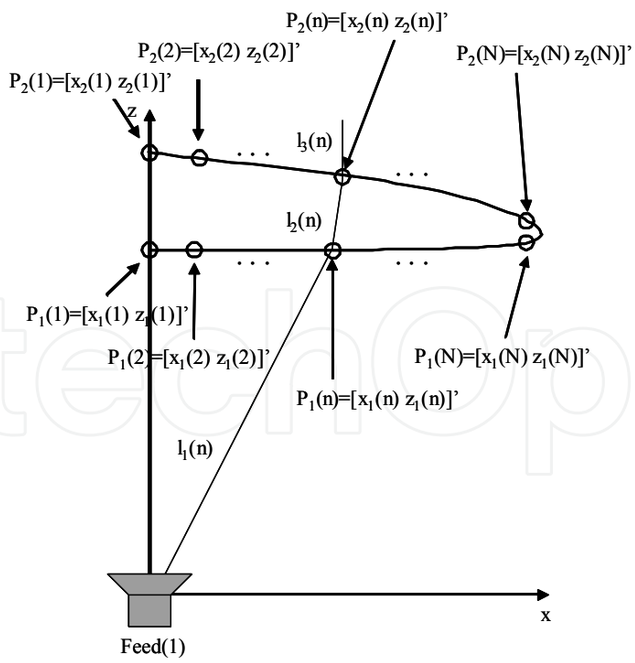

Fig. 3. The coordinate system for analysis

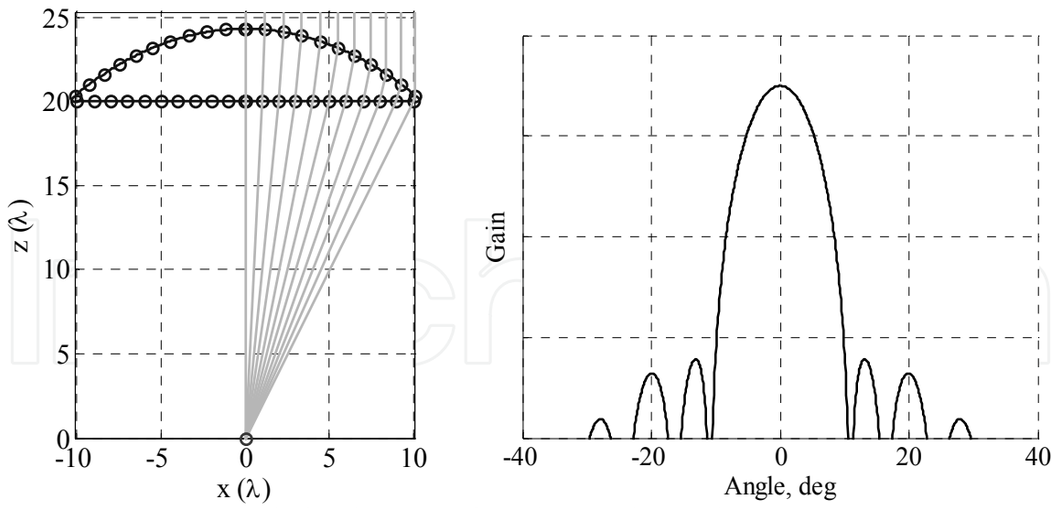

Fig. 4. Ray tracing example for the single focal lens and its radiation pattern

Then, we describe how to decide the focal points. $z_1(1)$ in $P_1(1)$ is determined so as to maximize the radiation efficiency. The radiation efficiency η of the space feed antenna is expressed by Eq.(8).

$$\eta = \frac{8}{\tan^2 \Phi} \frac{n_0 + 1}{(n_0 - 1)^2} \left\{ 1 - (\cos \Phi)^{\frac{n_0 - 1}{2}} \right\}^2 \tag{8}$$

The feed power pattern is assumed by,

$$D_0(\theta_0) = 2(n_0+1)\cos^{n0}(\theta_0) \tag{9}$$

where n_0 is a power index, and θ_0 is an angle from the centre axis. Φ is the angle between the z-axis and the line from the origin to the lens edge. When the aperture size is fixed, Φ is becomes a function of z, We assume $D_0(\theta_0)$ in both the E-plane and H-plane is the same. Fig.5 shows the radiation efficiency in case of n_0=20. When Φ=28°, η is maximized. $z_1(1)$ can be determined by the aperture radius and Φ.

(3)Bifocal lens

We briefly explain the design of a bifocal lens; the results of (Peebles, 1988) are used. $P_1(1)$ was determined so that the efficiency on the z-axis was maximized. The initial parameters, $P_1(1)$= 19.9λ, the thickness T_b=5.25λ and the scanning angle α=20° are given, all lens coordinates can be calculated iteratively. Fig. 6 shows a ray tracing example for the bifocal lens. First, $P_2(1)$ is determined by the Snell's law so that the ray direction from left focal point takes a after passing through the lens. Second, after a ray incident to $P_2(1)$ from -α is assumed, $P_1(2)$ is determined so as to arrive to right focal point through the lens. These procedures are carried out iteratively.

The focal point of xz-plane and yz-plane differs due to astigmatism. The focal point on the scanning plane is

$$R = F\cos^2(\theta) \ , \tag{10}$$

where F is focal length. The focal point on the transverse plane is

$$R = F. \tag{11}$$

The focal point of xz-plane and yz-plane differs due to astigmatism. Because the phase on the transverse plane is not considered, the radiation pattern may be degraded.

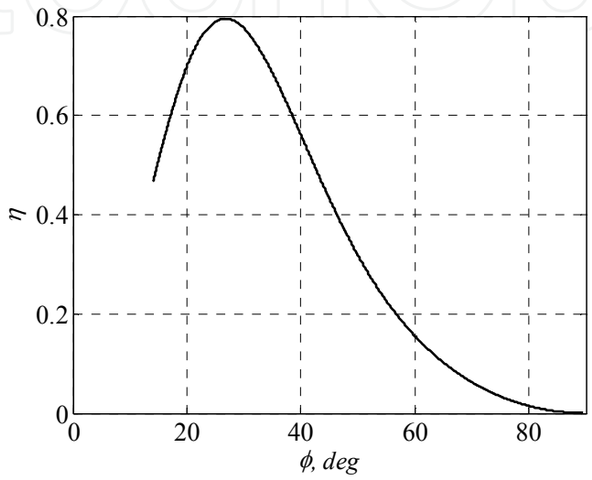

Fig. 5. Radiation efficiency (n_0=20)

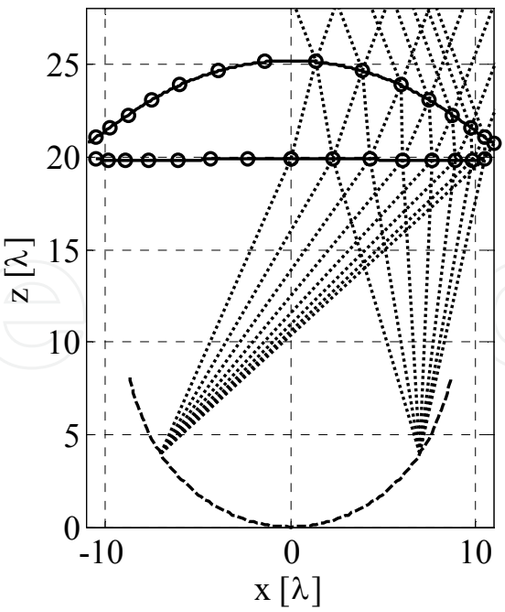

Fig. 6. Bifocal lens

3.2 Design of the lens for the multi-beam antenna

In this section, we discuss a multibeam antenna which forms 7 beams in the azimuth plane. The beam interval is 10^o. That is, the beam directions are -30^o, -20^o, …, 30^o. Our objective is to achieve several candidates for performance (gain and sidelobe level) trade off. Where, the lens structure is assumed to be rotating symmetry, and we examine 4 beams taking into account of symmetric multibeam in the azimuth plane.

(1)Design procedures

In our approach, the initial shape of lens is determined so as to yield a single focal lens. Next, the shape of the lens is modified so as to obtain the multibeam characteristics. The modifying values are given by the chromosomes. The positions of the feeds are also determined from the chromosomes. The radiation pattern of each structure is calculated and evaluated by the pareto ranking method. The individuals and the calculation procedure are shown in Fig. 7. The lens configuration considering the multibeam goal is also shown in Fig. 7.

First of all, $P_1(1)$ is defined.

$$P_1(1)=[0\ z_1(1)+\Delta z_1(1)]' \tag{12}$$

When Feed(1) is placed at the origin, $z_1(1)$ in $P_1(1)$ is determined so as to maximize the radiation efficiency. $z_1(1)$ is the value yielded by the maximization of the radiation efficiency. $\Delta z_1(1)$ is the correction value derived from the individuals. Though the optimized lens including $\Delta z_1(1)$ may not offer maximum efficiency, it offers better performance from the viewpoint of the multibeam characteristics.

The coordinates of the first plane that starts from $P_1(1)$ are determined. The interval, in the x-direction, of each $P_1(n)$ is constant, Δx_1. The difference, in the z-direction, from the previous point is defined as $\Delta z_1(n)$. Accordingly, $P_1(n)$ is expressed by the following recursion.

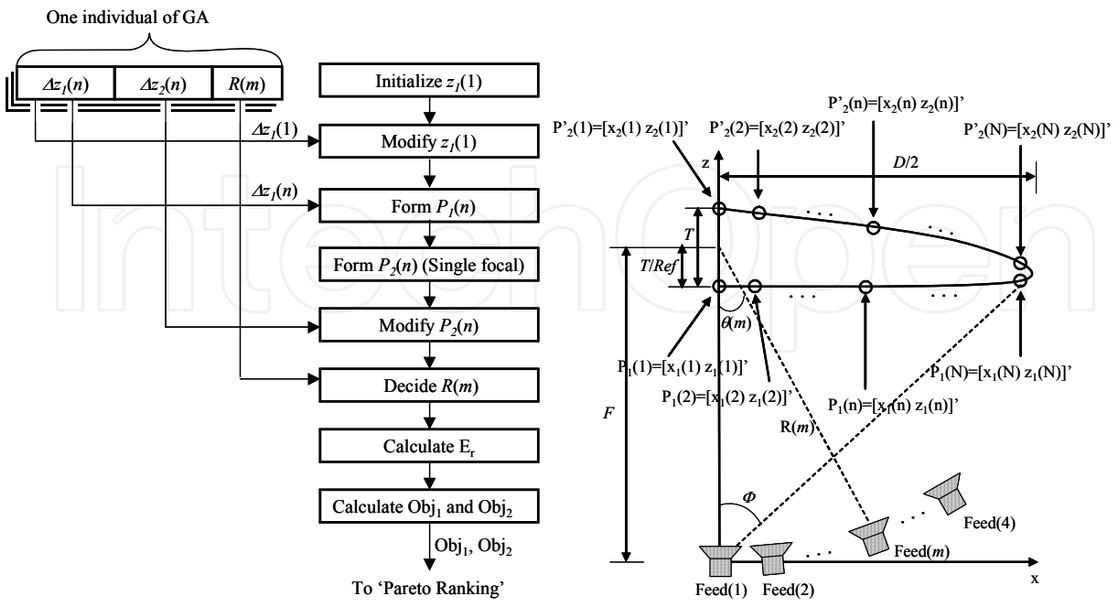

Fig. 7. Calculation procedure and lens configuration

$$P_1(n) = \begin{bmatrix} x_1(n-1) + \Delta x_1 \\ z_1(n-1) + \Delta z_1(n) \end{bmatrix} \qquad (2 \le n \le N) \tag{13}$$

$\Delta z_1(n)$ are derived from the individuals. Referring to $P_1(n)$, the coordinates of the second plane are determined so that a single focal lens can be formed. The criterion of the path length is satisfied when the ray from the feed (1) to $P_1(N)$ becomes parallel to the z-axis after refraction at the lens. Considering this path length and the refraction at the first plane, all $P_2(n)$ can be determined so that $l_e(x,y)$ is constant. The result is a single focal lens with modified first plane.

Next, $P_2(n)$ are modified to $P'_2(n)$ to obtain the desired multibeam characteristics. Similar to $P_1(n)$, $x_2(n)$ in $P_2(n)$ are unchanged and $z_2(n)$ are modified to $z'_2(n)$.

$$P'_2(N)=[x_2(N)\ z_2(N)+\Delta z_2(N)]^T \tag{14}$$

$$P'_2(n) = \begin{bmatrix} x_2(n) \\ z_2(n) + \Delta z_2(n) + z'_2(n+1) - z_2(n+1) \end{bmatrix} \quad (N-1 \ge n \ge 1) \tag{15}$$

$\Delta z_2(n)$ are also derived from the individuals. $\Delta z_2(n) + z'_2(n+1) - z_2(n+1)$ represents the accumulation of correction value from the lens edge. Equ.(15) can gradually change toward the lens centre. The result is a lens with both planes modified.

Feed (2) is placed on the line formed by $\theta(2) = 10^o$. When the lens thickness on z-axis is T, the intersection point between the z-axis and $R(m)$ is defined as T/ref from $P_1(1)$ (Rao, 1974). Feed (3) and Feed (4) are placed at 20 and 30 degrees, respectively. Each feed is directed to $P_1(1)$ to reduce the spillover. The focal lengths have yet to be determined. Because the focal point of xz-plane and yz-plane differs due to astigmatism, GA decides the focal lengths. The guesses of $R(m)$ are calculated from (Brown, 1956). The focal point on the scanning plane is

$$R(m)=F\cos^2(\theta(m)) \quad (m = 1 \cdots 4), \tag{16}$$

where F is the focal length shown in Fig. 7. The focal point on the transverse plane is

$$R(m)=F \quad (m = 1 \cdots 4), \tag{17}$$

From (16) and (17), the search range of feed locations is determined. The positions are also derived from the individuals to obtain better performance.

To evaluate the modified lens performance, the radiation patterns of the designed shapes are calculated by Equ.(6). Here, three cross sections for the pattern calculation are defined. They are shown in Fig.8, Fig.8(a) is the scanning plane pattern: $\varphi=0^o$ and θ is swept on the xz-plane. It is named $E_{rm}(\theta)$. Fig.8(b) is the transverse plane pattern: Θ_{90}, newly defined, is swept on the vertical plane from the xz-plane, including the maximum radiating direction as θ_m, $\theta_1=0^o$, $\theta_2=10^o$, and so on. It is named $Er_m(\Theta_{90})$. Fig.5(c) is the 45^o cut plane from the xz-plane, and includes the maximum radiating direction of each feed. It is named $Er_m(\Theta_{45})$.

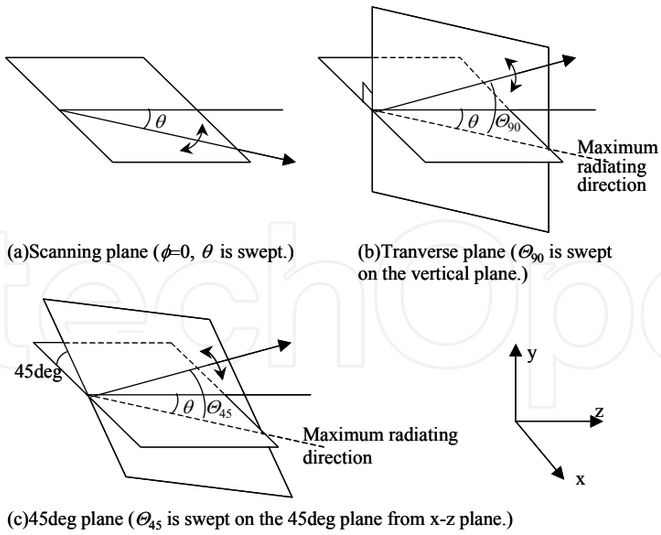

Fig. 8. Coordinate system for calculating the radiation pattern

Two objective functions for evaluating the obtained patterns $Er_m(\theta)$, $Er_m(\Theta_{90})$ and $Er_m(\Theta_{45})$are defined. The first object is the minimum gain on the desired angle θ_m (m=1,…,4) of each feed.

$$Obj_1=\min[Er_m(\theta_m)] \quad (m=1\cdots4) \tag{18}$$

The second object is the minimum value of the ratio between the gain and the sidelobe level (SLL).

$$Obj_2=\min[Er_m(\theta_m)/SLL(Er_m(\theta)) \;\; Erm(\theta_m)/SLL(Er_m(\Theta_{90})) \;\; Er_m(\theta_m)/SLL(Er_m(\Theta_{45}))]$$

$$(m=1\cdots4) \tag{19}$$

SLL(·) represents the calculated value of the maximum sidelobe level. The shoulder of the mainlobe at which the polarity of 2nd order difference for directivity change is included in this sidelobe level. The first element in Equ.(19) represents the ratio on the scanning plane. The second element represents the ratio on the transverse plane. The third element represents the ratio on 45°cut plane. Equ. (18) and (19) are evaluated for all individuals.

Though we calculated the results using Equ. (18) and (19), lens configuration satisfying other performance requirements can be achieved by changing or adding objective functions; for example, the objective function for every feed can be defined individually, the sidelobe condition is defined on the scanning plane and the transverse plane separately instead of Equ.(19), or the beamwidth is defined as the objective function.

(2)Numerical simulation

A. Simulation Model

The validity of the proposed method is demonstrated in this section. The simulation conditions are shown in Table 1. The lens coordinates on the *x*-axis are defined up to 10.5λ to obtain accurate refraction at the lens edge, i.e., *N* is set to 22.

Calculation of all possible combinations of the chromosomes is impractical since 2^{376} combinations (about 10^{113}) would have to be assessed. On the other hand, our procedure with GA yields improved performance quickly. Mutation probability was gradually reduced by the convergence of the results. The radiation pattern of the feed with the normalized gain of 0dB is shown in Fig. 9. The two broken lines represent the lens edges for Feed (1) in Fig. 7.

Elements	Values
Lens aperture diameter D	20λ
Refractive index Ref	1.6
Interval of $x_1(n)$ (=Δx_1)	0.5λ
Number of $x_1(n)$ N	22
Range of $\Delta z_1(1)$	$\pm 1\lambda$
Range of $\Delta z_1(n)$ $(n \neq 1)$, $\Delta z_2(n)$	$\pm 0.05\lambda$
Distance between lens and feed $R(m)$	Min: $F\cos(\theta(m))$ Max: F
Exponential index of feed n_0	20
Initial coordinate of first plane $z_1(1)$	19.9λ
Number of individual	40
Number of elements composing one individual	47 (22 for $P_1(n)$, 22 for $P_2(n)$, 3 for $R(m=2,3,4)$)
Number of bits for each element	8 (256 levels)
Number of bits in one individual	376 (=47×8)
Number of generations	100
Mutation probability	Start: 0.2 End: 0.1
Crossover probability	0.01

Table 1. Simulation conditions

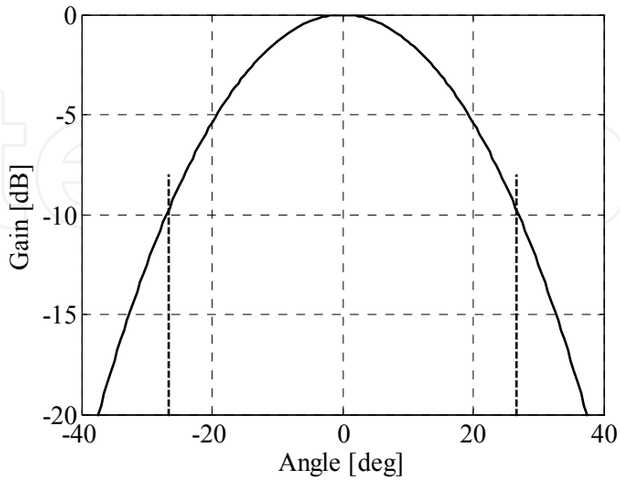

Fig. 9. Characteristics of the feed

B. Results

The calculation result is shown below. The values of objective functionsEqu. (18) and (19) at the final generation are shown in Fig. 10. The circles in this figure represent each individual's performance. The asterisk shows the performance of the bifocal lens with the same diameter lens and feed characteristics. From Fig. 10, we can see that the pareto-optimal solutions offer high gain and/or low sidelobe level and each individual was diffused.

Individual A in Fig. 10 is pareto-optimal. It has almost the same sidelobe level as the bifocal lens and its gain is improved by 1.7dB. It has well balanced characteristics. Individual B is also pareto-optimal. Its design targeted the sidelobe level. Though it seems that the sidelobe level was lowered from the bifocal lens in our criterion, the sidelobe performance is almost the same with the bifocal lens for practical use. This is explained later by using the radiation pattern. Individual C, also pareto optimal, was designed for enhanced gain. These characteristics are listed in Table 2.

1)Individual A : With regard to individual A, the lens shape and the radiation pattern are demonstrated. The lens shape and feed positions are shown in Fig. 11. The lens shape was almost plano-convex. The radiation patterns in the scanning plane, the transverse plane and 45deg-cut plane are shown in Fig. 12, respectively. Solid lines are the characteristics of the proposed lens. Broken lines are for the bifocal lens. In figures for the transverse plane and 45deg-cut plane, each feed was offset by 10 degrees, and the original peak occurs at Φ=0deg. Note that the patterns of each feed are not on the same plane. θ of each feed is rotated as shown in Fig. 8. The radiation pattern on the 45deg-cut plane had characteristics

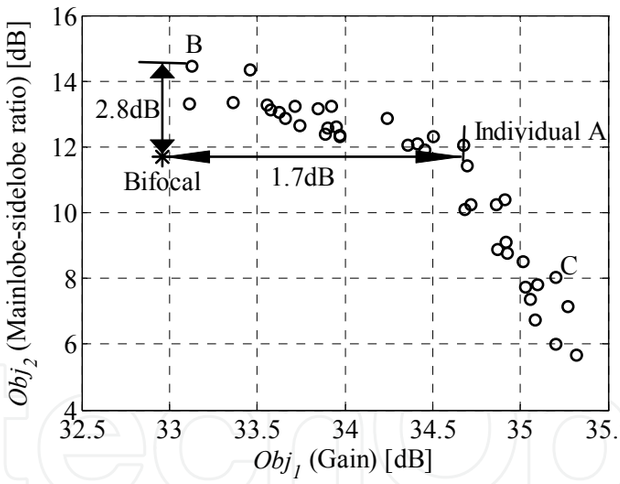

Fig. 10. Two objective functions at final generation

Individual	Obj_1	Obj_2
A	***34.7***	12.1
B	33.1	***14.5***
C	***35.2***	8.0
(Bifocal)	33.0	11.7

Table. 2. Characteristics of three individuals and bifocal lens

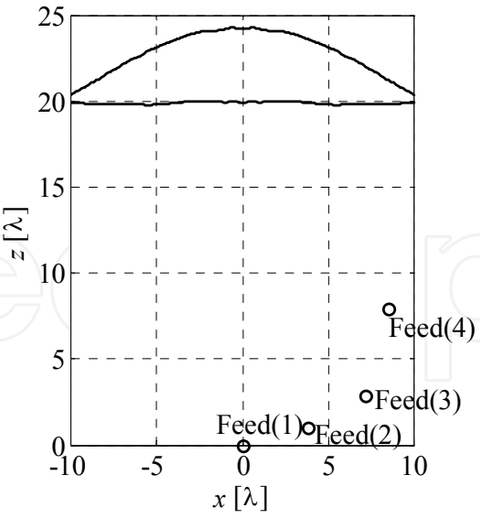

Fig. 11. Lens shape and feed position of individual A

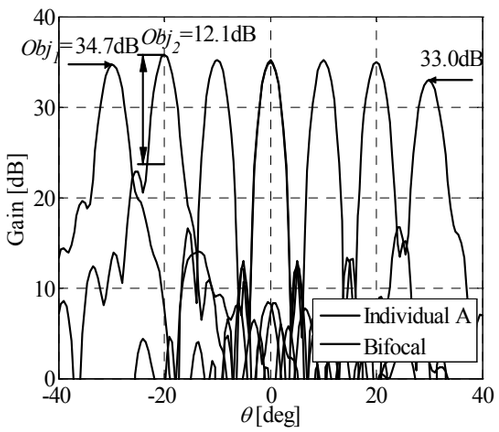

(a) Scanning plane

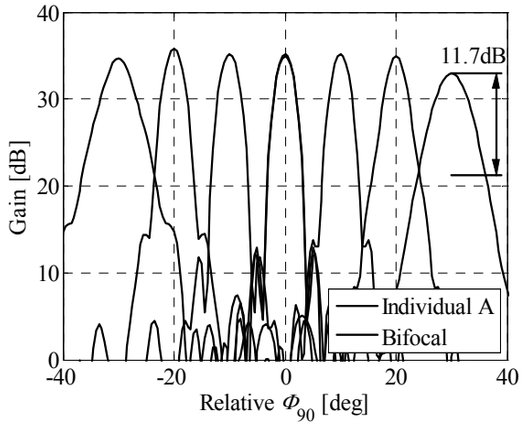

(b) Transverse plane

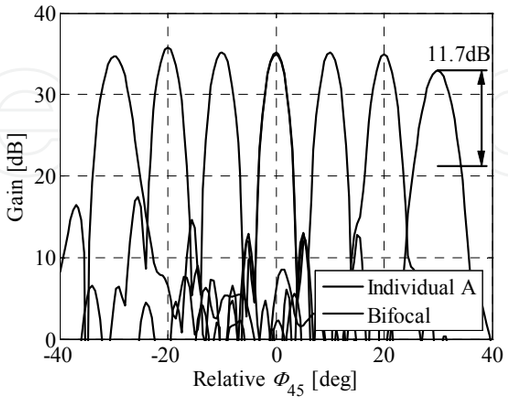

(c)45°cut plane

Fig. 12. Radiation pattern of individual A

intermediate between those on the scanning plane and those on the transverse plane. Obj_2 for individual A appeared in the radiation pattern of feed(3) on the scanning plane. On the other hand, that of the bifocal lens appeared in the radiation pattern of feed(4) on the transverse plane. In both cases, the small shoulder of the mainlobe was detected as the sidelobe. While the sidelobe level is almost the same, the gain of the proposed lens is significantly improved.

2)Individual B : With regard to individual B, the lens shape and the feeds position and the radiation pattern are shown in Fig. 13 to 14, respectively. The pattern on the 45deg-cut plane was omitted because Obj_2 did not appear on the plane. Individual B was designed for improved sidelobe level. Obj_2 appeared in the radiation pattern of feed (4) on the transverse plane. Compared to the bifocal lens, it seems to have almost the same gain and improved sidelobe level. The worst sidelobe level in the case of bifocal lens is always identified as a shoulder in the main lobe. The shoulder is very difficult to identify by visual inspection

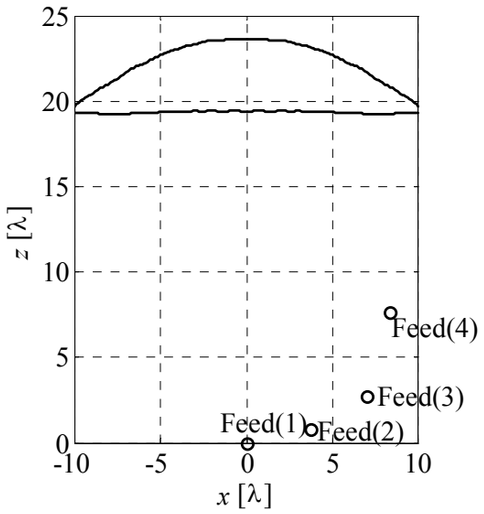

Fig. 13. Lens shape and feed position of individual B

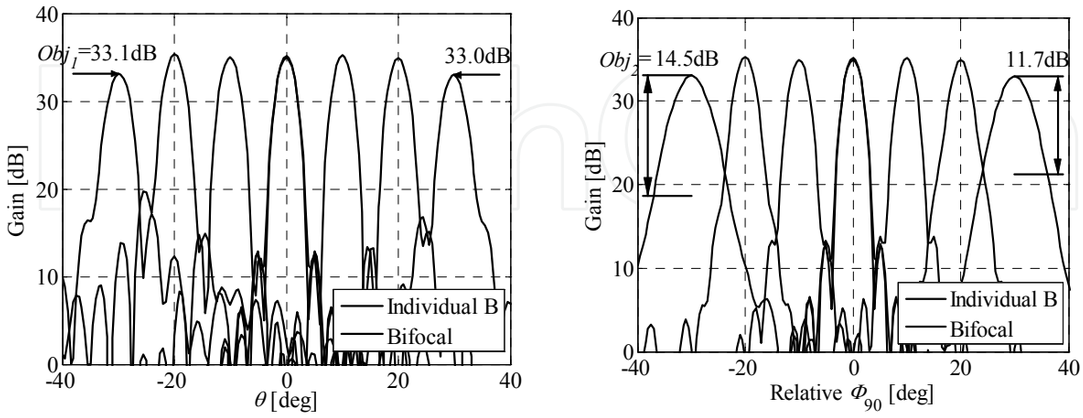

(a) Scanning plane (b) Transverse plane

Fig. 14. Radiation pattern of individual B

since it is associated to a 2nd order polarity change for directivity. Such a sidelobe on that beam is not very dangerous for practical use.
3)Individual C : With regard to individual C, the lens shape and the radiation pattern are shown in Fig. 15 to 16, respectively. In exchange for a rise of the sidelobe level in feed(4), the gain of feed(4) is improved up to the same extent as the other feeds.

3.3 Design for the collision avoidance radar antenna

In this section, we examine the collision avoidance radar. In order to avoid detecting miss due to the road inclination, it is necessary to form vertical fan beam. Also, in order to detecting miss in the azimuth plane, it is necessary to overlap adjacent 2 beams. That is, we should reduce the pattern loss. Fig. 17 shows the requirements in this case. Each feed is placed at interval of 10^{o}. The negative side display is symmetrical and so is omitted.

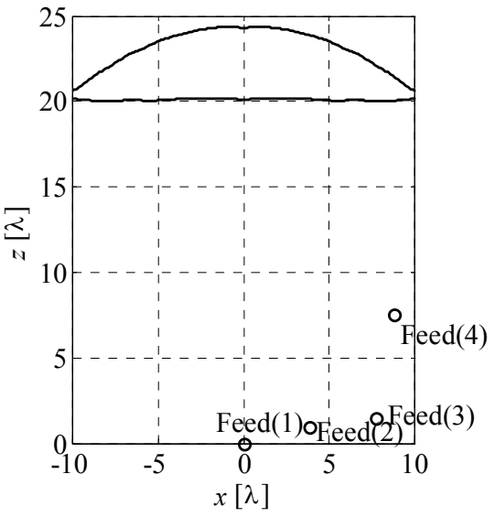

Fig. 15. Lens shape and feed position of individual C

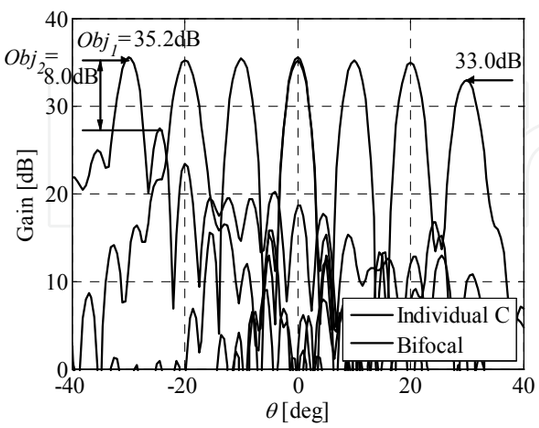

(a) Scanning plane

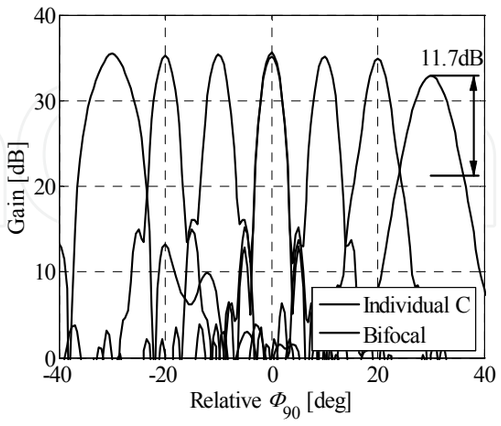

(b) Transverse plane

Fig. 16. Radiation of individual C

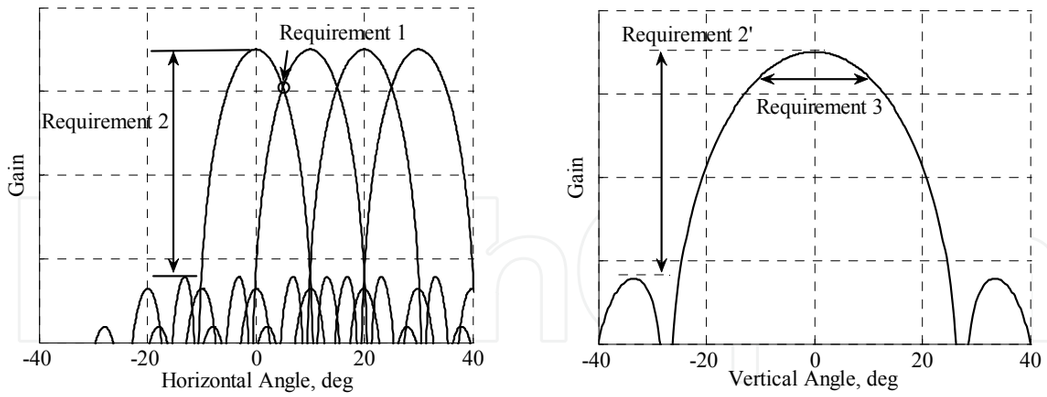

(a) Azimuth pattern (b) Elevation pattern

Fig. 17. Requirements of the radiation pattern

First requirement is high gain including pattern loss; the gain should be as large as possible. This can achieve by using a large aperture but this narrows the beamwidth. If the beamwidth was smaller than that shown in Fig.17(a), deep nulls may appear at intermediate angles between the peaks; 5^o,15^o and 25^o. This must be avoided because it could lead to the failure to detect targets. Accordingly, it is preferable that the mainlobes created by adjacent feeds overlap. Because the minimum detection sensitivity is determined by the gain at the overlap point rather than maximum gain, we aim to maximize the gain at the overlap angle. This is shown in Fig. 17(a), Requirement 1. This value is determined by the aperture size, focal length and radiation pattern of the feed. The second requirement is the suppression of the sidelobe level, see Fig. 17(a), Requirement 2. This requirement can be satisfied by tapering the electric field of the aperture, which reduces the edge taper level. This technique can be realized by moving the feed array closer to the lens or narrowing the beam of each feed. However, the gain and/or radiation efficiency should be considered. The requirement in the elevation plane is similar to that in the azimuth plane, see Fig. 17(b), Requirement 2'. The beamwidth in the elevation plane is the third requirement, see Fig. 17(b), Requirement 3. A certain value is required to ensure adequate coverage in the vertical plane. Because the beamwidth and the gain conflict, these requirements should be balanced.

(1) Design procedures

Basic procedure is the same as preceding section. However, in order to form the vertical fan beam, the aperture is cut off elliptically. Therefore, the minor and major axis are added to chromosomes as new gene. The chromosome structure, calculation procedure and lens configuration are shown in Fig. 18.

In this case, $P_1(1)$ is also defined by chromosome. Because it is considered that the optimum focal length exists on the midpoint between the optimum for the circular aperture with major axis and that with the minor axis.

$$P_1(1)=[0\ z_1(1)+\Delta z_1(1)]^T \tag{20}$$

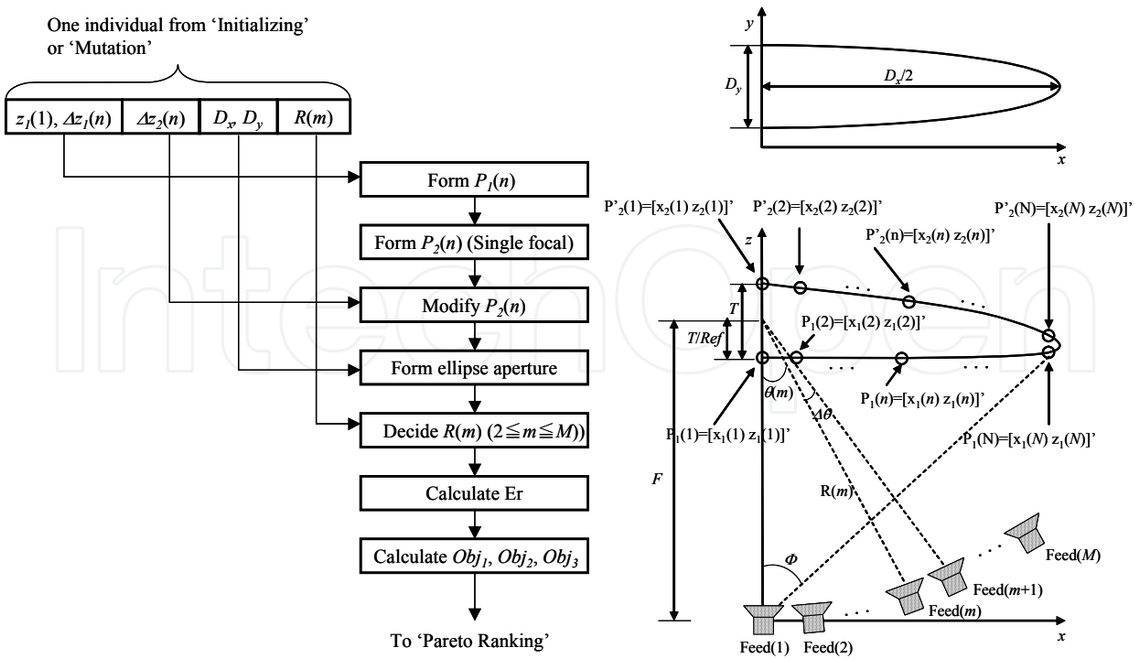

Fig. 18. Calculation procedure and lens configuration

$\Delta z_1(1)$ is the correction value derived from the individuals. Applying $\Delta z_1(1)$ can yield superior results in multibeam antenna design. The coordinates of the first plane that starts from $P_1(1)$ are determined. The interval, in the x-direction, of each $P_1(n)$ is constant, Δx_1. The difference, in the z-direction, from the previous point is defined as $\Delta z_1(n)$. Accordingly, $P_1(n)$ is expressed by the following recursion.

$$P_1(n) = \left[x_1(n-1) + \Delta x_1 \quad z_1(n-1) + \Delta z_1(n)\right]^T \qquad (2 \le n \le N) \tag{21}$$

$\Delta z_1(n)$ are derived from the individuals. Referring to $P_1(n)$, the coordinates of the second plane $P_2(n)$ are determined so that a single focal lens can be formed. The result is a single focal lens with modified first plane. Next, $P_2(n)$ are modified to $P'_2(n)$ to obtain the desired multibeam characteristics. Similar to $P_1(n)$, $x_2(n)$ in $P_2(n)$ are left and $z_2(n)$ are modified to $z'_2(n)$.

$$P'_2(N)=[x_2(N)\ z_2(N)+\Delta z_2(N)]^T \tag{22}$$

$$P'_2(n) = \left[x_2(n) \quad z_2(n) + \Delta z_2(n) + z'_2(n+1) - z_2(n+1)\right]^T \qquad (N-1 \ge n \ge 1) \tag{23}$$

$\Delta z_2(n)$ are also derived from the individuals. By rotating the cross section made by $P_1(n)$ and $P_2(n)$ around z axis, form of lens is achieved.

Feed (2), (3), (4) are placed on the line formed by θ(2) = 10˚, 20˚ and 30˚, respectively. Each feed is directed to $P_1(1)$ to reduce the spillover. The focal lengths are also derived from the individuals to obtain better performance.

To investigate the beam width in the elevation plane and the pattern loss in the azimuth plane, the major axis D_x, and the minor axis D_y of the lens are incorporated into the chromosome as the gene.

To evaluate the modified lens performance, the radiation patterns of the designed shapes $E_{rm}(\theta, \phi)$ are calculated. The patterns from $E_{r1}(\theta, \phi)$ to $E_{r4}(\theta, \phi)$ correspond to each feed. Here three objective functions are defined. The first object is the minimum gain where two beams intersect.

$$Obj_1=\min[E_{rm}(\theta_{cross}(m), 0)] \quad (m = 1 \cdots 3) \tag{24}$$

$\theta_{cross}(m)$ is an angle intersecting mth beam with m+1th beam. The second object is the minimum value of the ratio between the gain and the sidelobe level.

$$Obj_2=\min[E_{rm}(\theta(m), 0)/SLL(E_{rm}(\theta, 0)) \;\; E_{rm}(\theta(m), 0)/SLL(E_{rm}(\theta(m), \varphi))] \quad (m = 1 \cdots 4) \tag{25}$$

SLL(·) represents the calculated value of the maximum sidelobe level. The first half of Equ.(25) represents the multibeam pattern in the azimuth plane. The second half of Equ.(25) represents the fan beam pattern in the elevation plane. Here, evaluation on 45°cut-plane described in the preceding section is omitted, since the maximum sidelobe must not appear on 45°cut-plane. The third object is formation of sector beam in the elevation plane. Here, it is assumed to form beamwidth of 20˚.

$$Obj_3=\min[\,-|\phi_{3dB}(m)-20|\,] \quad (m = 1 \cdots 4) \tag{26}$$

$\phi_{3dB}(m)$ is beamwidth of vertical pattern of mth beam. Equ. (24), (25) and (26) are evaluated for all individuals.

(2) Feed design

In the past, we used the Vivaldi slot line (Yun & Chang, 2001) antenna as the feeds. However, there were some drawbacks as sidelobe, beamwidth, and pattern symmetry. We have tried to use the Fermi antenna with corrugation (Sugawara et al., 1998) as the feeds. It is featured by low sidelobe, good symmetric radiation pattern and wide frequency range.

Configuration of the antenna is shown in Fig. 19. The antenna has taper slot represented by Fermi function and corrugation at both sides. Fermi function is expressed by

$$f(x) = \frac{a}{1 + e^{-b(x-c)}} \tag{27}$$

Where, a, b and c are parameters that determine the taper.

We have examined design parameters, that is, Fermi function, aperture width, antenna length, corrugation pitch, and corrugation depth by FDTD. The design policies are large difference between beamwidth of the elevation and azimuth plane, low sidelobe, good symmetric radiation pattern and impedance. We have used Diclad 522 which thickness is 0.8mm and the dielectric constant is 2.6 as the substrate. The designed configuration is shown in Fig. 20. Parameters in Equ.(27) are a=4[mm] , b=0.048, c=25[mm] . The radiation pattern is shown in Fig. 21. The VSWR was lower than 2.7 from 20 to 27GHz. Beamwidth of the azimuth and elevation plane is 36° and 30°, respectively. Sidelobe level of the azimuth and elevation plane is -13 and -19dB, respectively.

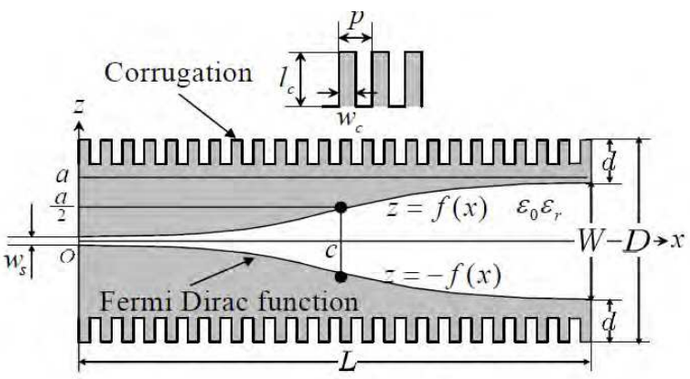

Index	value
a	12.75
b	50
c	5.25
d	8.25
e	1
f	0.25
lc	2
g	3
h	3.5
i	1
j	6.5

Fig. 19. Fermi antenna with corrugation

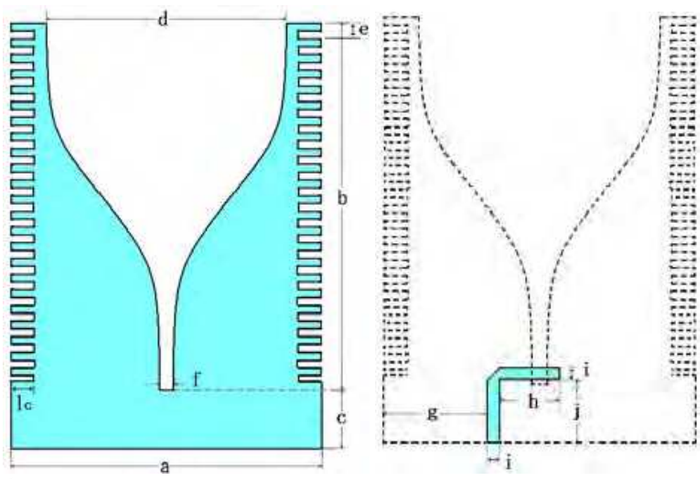

Fig. 20. Design results

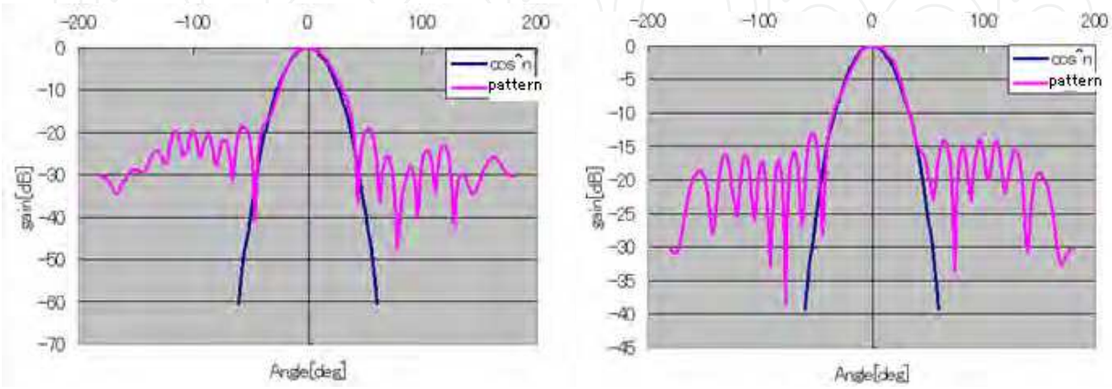

elevation plane(n_E=20) azimuth plane(n_H=13)

Fig. 21. Radiation pattern and $\cos^n \theta$ approximation

(3) Numerical simulation

A. Simulation model

A design obtained by the proposed method is demonstrated in this section. The calculation conditions are shown in Table 3. We assumed the feed pattern as power of cosine function as shown in Fig. 21. The power index in Equ.(9) are n_E=20 or n_H=13. The radiation pattern of the feed is modified.

$$D_0(\theta_E, \theta_H) = 2\sqrt{(n_E+1)(n_H+1)}\cos^{n_E}\theta_E \cos^{n_H}\theta_H \tag{28}$$

In order to calculate the refraction at the lens edge accurately, the lens was formed up to +0.5λ from D_x and D_y and ray tracing was carried out up to D_x and D_y. Mutation probability is gradually reduced by the convergence of the results. Crossover probability is set at a relatively low value because mutation with elitist preserving selection yielded better performance rather than crossover. Calculation of all possible combinations of the chromosomes is impractical since 2^{392} combinations (about 10^{118}) would have to be assessed. Considering calculation loads, our procedure with GA is far more practical.

Elements	Values
Direction interval of feeds, $\Delta\theta$	10°
Power index of the feed, n	n_E=20, n_H=13
Range of aperture diameter, D_x, D_y	1.5 to 9λ
Range of lens offset against feed(1), $z_1(1)$	1 to 12λ
Interval of $x_1(n)$ (=Δx_1)	0.5λ
Range of $\Delta z_1(n)$and $\Delta z_2(n)$	$\pm 0.05\lambda$
Distance between lens and feed $R(m)$	$F\cos(\theta(m))$ to F
Refractive index, *Ref*	1.6
Number of individual	50
Number of elements composing one individual	49 (D_x, D_y, $z_1(1)$, $\Delta z_1(n)$x21, $\Delta z_2(n)$ x 22, $R(m)$ x 3)
Number of bits for each element	8 (256 levels)
Number of generations	100
Mutation probability	Start : 0.2 End : 0.1
Crossover probability	0.01

Table 3. Simulation conditions

B. Results

A calculation result is shown below. The values of objective functions Equ.(24), (25) and (26) at the final generation are shown in Fig. 22. The increasing extent of each axis represents superior performance. The circles in this figure represent each individual's performance. We can see that pareto-optimal solutions with various characteristics were obtained. The design specialized for one object yielded relatively decreased values in other objective functions. On the other hand, when the restriction of Obj_1 was reduced, design parameters yielding improvements in Obj_2 and Obj_3 were obtained. Considering balance between objective functions, we have selected the filling individual in Fig. 22. The lens shape and feed positions are shown in Fig. 23. The radiation patterns in the azimuth and elevation planes are shown in Fig. 24.

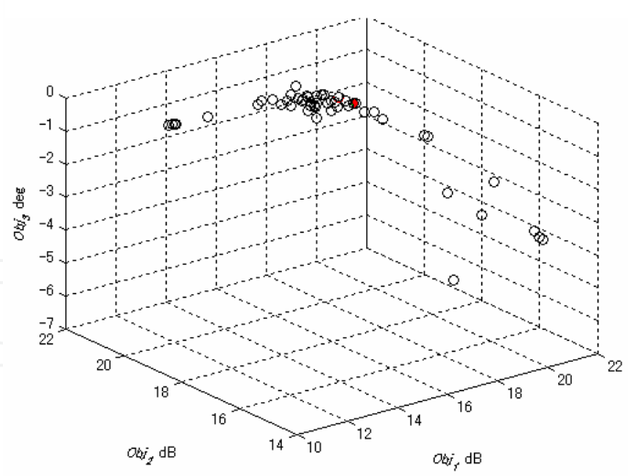

Fig. 22. distribution of the results

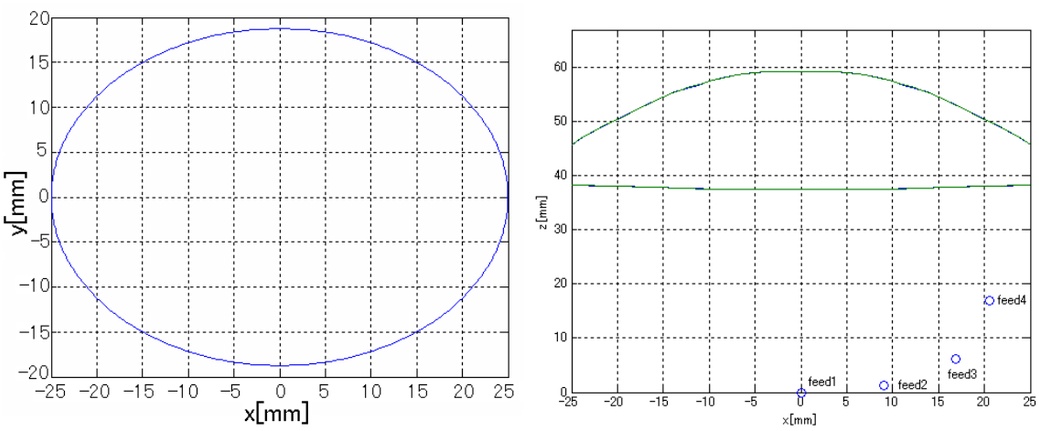

Fig. 23. Antenna configuration (f=24GHz)

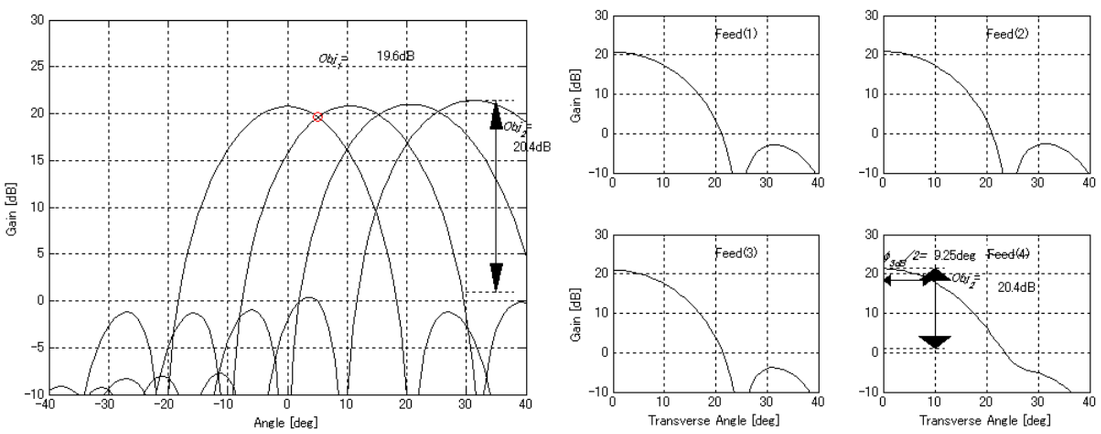

(a) azimuth plane (b) elevation plane

Fig. 24. Radiation patterns in the

4. Trial model and evaluation

We have manufactured a trial model based on the feed shown in Fig.20 and antenna configuration shown in Fig.23.

4.1 Feed

We have manufactured the trial model and have evaluated the performance. The trial model and the measured VSWR are shown in Fig.25. The VSWR is lower than 2.4 from 20 to 27GHz. The radiation patterns are shown in Fig.26. Beamwidth of the horizontal and vertical plane is 35° and 29°, respectively. Sidelobe level of the horizontal and vertical plane is -12 and -15dB, respectively. These values are almost same as the numerical simulation results.

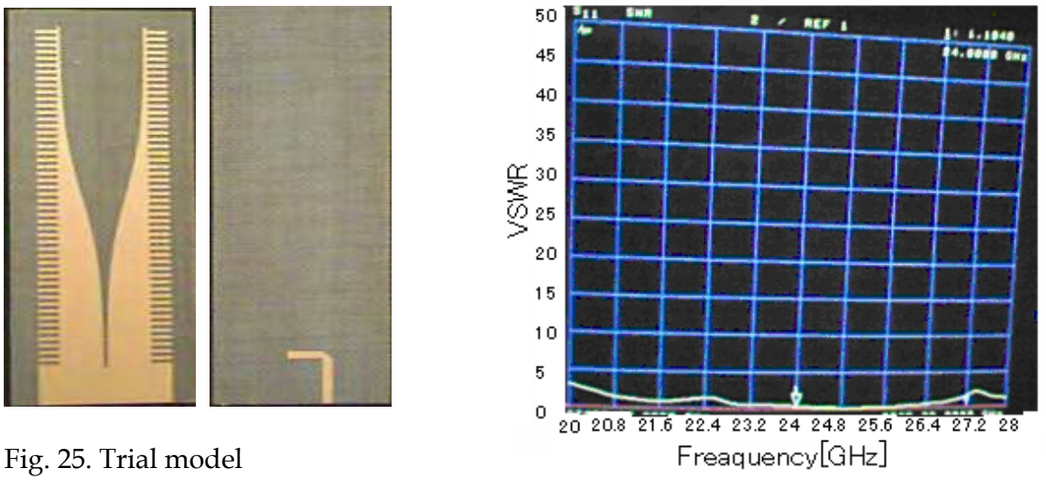

Fig. 25. Trial model

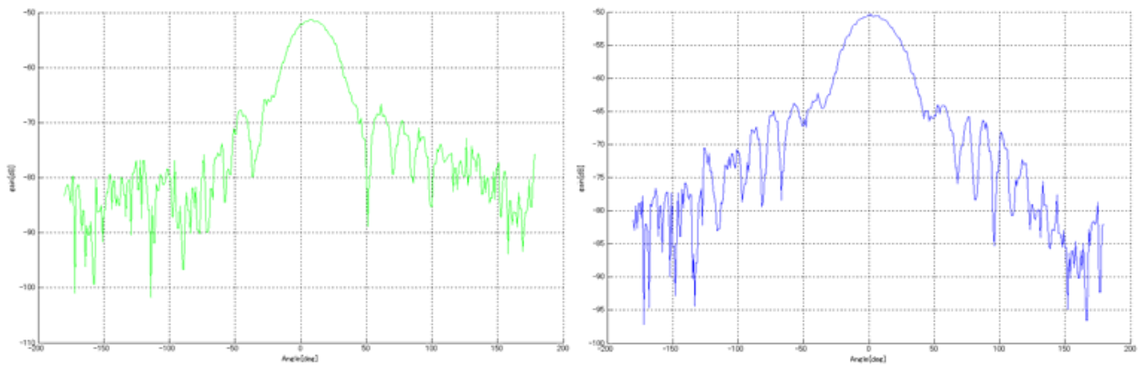

Elevation-plane Azimuth-plane

Fig. 26. Measured Radiation Pattern

4.2 Multibeam lens antenna

We have manufactured a trial model. Lens shape is shown in Fig.27. 3 arms are used for installation. The top view of whole structure is shown in Fig.28. Since we have confirmed that the aperture center of Fermi antenna is on the tips by phase pattern measurements, the tips are placed on the focal positions.

The measured radiation patterns are shown in Fig.29. The peak gain is 18 to 21dB, and inequality between multibeams is observed. The inequality is because of manufacturing error of the feed. The sidelobe level is -10 to -14dB. It is considered that the sidelobe rises up by interference between the feeds. The shoulders along the mainbeam are also observed. The shoulders are appeared by interference between the feeds and reflection of the antenna structure. The vertical beamwidth is 18°. It is almost the same value of the design. We were not able to measure the sidelobe in the vertical plane due to limitations of measuring system.

top view back view side view

Fig. 27. dielectric lens

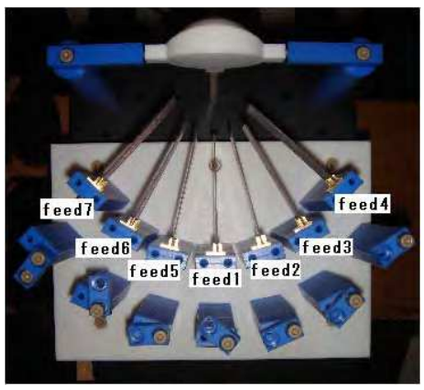

Fig. 28. Whole structure (Top view)

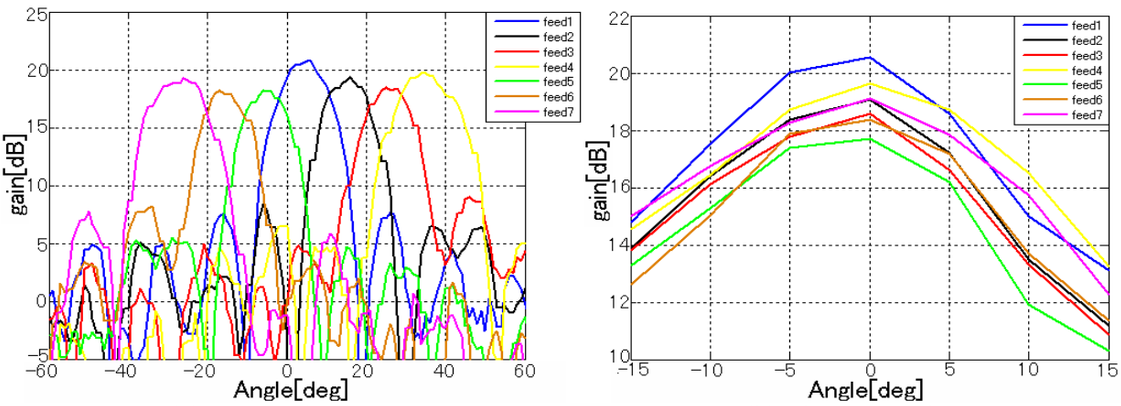

(a) Azimuth plane (b) Elevation plane

Fig. 29. measured pattern

5. Conclusions

We have proposed the design scheme for multibeam dielectric lens antennas that well balances the conflicting aims of high gain and low sidelobe level. The scheme is based on pareto-GA and lens shape is associated with GA chromosomes.
In the first, two objective functions are defined: the gain and the sidelobe level. Individuals are renewed yielding pareto optimal solutions that identify various lens shape. Some examples of lens shape and their radiation patterns were demonstrated by numerical simulation. Our design scheme provides various forms that offer well balanced performance including the gain-tuned lens and the sidelobe level tuned lens.
Second, as an example of 3 objectives, multibeam dielectric lens antennas with the fan beam has examined. To optimize the lens antennas balancing the gain including pattern loss of multibeam and sidelobe level of the scanning and transverse patterns taking into account of beamwidth of the vertical pattern, the pareto-genetic algorithm is successfully introduced. The validities have been confirmed by numerical simulation.
Then, Fermi antenna with corrugation has been examined for feed. We have confirmed the good performances of Fermi antennas with corrugation for the feed at 24GHz band through trial manufacturing and evaluation tests. And, trial model has been manufactured and evaluated. Although we were able to confirm certain degrees of performance, the evaluation results were not satisfied with our goals. The main problem is interference between feeds. We confirmed that the performance were dramatically improved when feeds separated away. Therefore, we are to design with constrain of focal length. Of course, the feed pattern must be examined.

6. References

Y. Kuwahara, M. Hamai, and T. Maruyama, "Multi-beam antenna with vertical fan beam of the dielectric lens and Fermi antennas with corrugation," *in Proc. 2009 IEEE int. symposium on antennas and propagation*, 426.6, June 2009.

T. Maruyama, K. Yamamori, and Y. Kuwahara, "Design of multibeam dielectric Lens antennas by multi-objective optimization," *IEEE Trans. Antennas and Propagat.*, Vol.57 No.1, pp.57-63, Jun. 2009.

Y. Kuwahara, "Design of multibeam dielectric Lens antennas with the fan beam by multi-objective optimization," *Proc. of ISAP 2008,* 1645103, Oct. 2008.

B. L. J. Rao, "Bifocal dual reflector antenna," *IEEE Trans. Antennas Propagat.*, Vol. 22, No. 5, pp. 711-714, Sept. 1974.

R. M. Brown, "Dielectric bifocal lenses," *IRE International Conv. Rec.*, pp.180-187, Mar. 1956.

A. L. Peebles, "A dielectric bifocal lens for multibeam antenna applications," *IEEE Trans. Antennas Propagat.*, Vol.36, No. 5, pp. 599-606, May. 1988.

R. K. Luneburg, *Mathematical Theory of Optics*, Univ. of California Press, 1964.

E. E. Altshuler and D. S. Linden, "Wire-antenna designs using genetic algorithms," *IEEE Antennas Propagat. Mag.*,Vol. 39, No. 2, pp. 33-43, Apr. 1997.

E. A. Jones and W. T. Joines, "Design of Yagi-Uda antennas using genetic algorithms," *IEEE Trans. AntennasPropagat.*, Vol. 45, No. 9, pp. 1386-1392, Sept. 1997.

Y. Kuwahara, "Multiobjective optimization design of Yagi-Uda antenna," *IEEE Trans. Antennas Propagat.*, Vol. 53, No. 6, pp. 1984-1992, June. 2005.

C. M. Fonseca and P. J. Fleming, "Genetic algorithms for multiobjective optimization: Formulation, discussion and generalization," in *Proc. 5th Int. Conf. Genetic Algorithm*, 1993, pp. 416-423.

R. L. Haupt and S. E. Haupt, "Practical Genetic Algorithms," Wiley-Interscience, New York, ISBN 0-471-18873-5, 1998.

Y. Rahmat-Samii and E. Michielessen, "Electromagnetic Optimization by Genetic Algorithms," Wiley-Interscience, New York, ISBN 0-471-29454-0, 1999.

D. H. Werner and R. Mittra, "Frontiers in Electromagnetics," IEEE Press, New York, ISBN 0-7803-4701-3, 2000.

E. E. Alshuler and D. S. Linden, "Wire-Antenna Designs Using Genetic Algorithms," *IEEE Antennas and Propagat. Magazine*, Vol. 39, No. 2, pp.33-43, Apr. 1997.

D. S. Weile, E. Michielssen, and D. E. Goldberg, "Genetic Algorithm Design of Pareto Optimal Broadband Microwave Absorbers," *IEEE Trans. on Electromagnetic Compatibility,* Vol. 38, No. 3, pp.518-525, Aug. 1996.

D. S. Weile and E. Michielssen, "Genetic Algorithm Optimization Applied to Electromagnetics: A Review," *IEEE Trans. Antennas Propagat.*, Vol. AP-45, No. 3, pp.343-353, Mar. 1997.

D. S. Weile and E. Michielssen, "Integer coded Pareto genetic algorithm design of constrained antenna arrays," *Electronics Letters,* Vol. 32, No. 19, pp.1744-1745, 1996.

S. E. Fisher, D. S. Weile, and E. Michielssen, "Pareto Genetic Algorithm Based Optimization of Log Periodic Monopole Arrays Mounted on Realistic Platforms," *Journal of Electromagnetic Waves and Applications*, Vol. 13, pp.571-598, 1999.

H. Choo and H. Ling, "Design of electrically small planar antennas using inductively coupled feed," *Electronics Letters*, Vol. 39, No. 22, pp.1563-1565, 2003.

J. Horn, N. Nafpliots, and D. E. Goldberg, "A Niched Pareto Genetic Algorithm for Multiple Objective Optimization," Proc. of *the 1st IEEE Conf. Computation*, pp.82-87, 1994.

K. A. D. Jong, "An Analysis of the Behavior of a Class of Genetic Adaptive Systems," Doctoral dissertation, University of Michigan, 1975.

J. D. Scaffer, "Multiple objective optimization with vector evaluated genetic algorithm," Proc. of *the 1st International Conference on Genetic Algorithm and their Applications*, pp.160-168, 1985.

Y. Tajima, Y. Yamada, S. Sasaki, A. Kezuka, "Calculation of Wide Angle Radiation Patterns and Caustics of a Dielectric Lens Antenna by a Ray Tracing Method," *IEICE Trans.* Elec., vol. E87-C, No.9, pp. 1432-1440, Sept. 2004.

J.J.Lee, Handbook of Antenna Theory and Design, Chapter. 16, Van Nostrand Reinhold Co, New York, 1988.

Y. Kuwahara, T. Ishita, Y. Matsuzawa, and Y. Kadowaki, "An X-band phased array antenna with a large elliptical aperture," *IEICE* Trans. Commun., vol. E76-B, no. 10, pp. 1249-1257, Oct. 1993.

T. Yun and K. Chang, "A Low Cost 8 to 26.5GHz Phased Array Antenna Using a Piezoelectric Transducer Controlled Phase Shifter," I*EEE Trans. on Antennas and Propagation*, vol49, no.5, pp.1290-1298, Sep. 2001.

S. Sugawara, Y. Maita, K.Adachi, K. Mori and K. Mizuno," Characteristics of a MM-wave Tapered Slot Antenna with Corrugated Edges," *1998 MTT-S Digest*, pp.533-536, 1998.

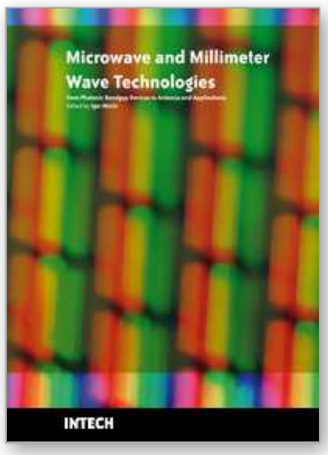

Microwave and Millimeter Wave Technologies from Photonic Bandgap Devices to Antenna and Applications

Edited by Igor Minin

ISBN 978-953-7619-66-4
Hard cover, 468 pages
Publisher InTech
Published online 01, March, 2010
Published in print edition March, 2010

The book deals with modern developments in microwave and millimeter wave technologies, presenting a wide selection of different topics within this interesting area. From a description of the evolution of technological processes for the design of passive functions in milimetre-wave frequency range, to different applications and different materials evaluation, the book offers an extensive view of the current trends in the field. Hopefully the book will attract more interest in microwave and millimeter wave technologies and simulate new ideas on this fascinating subject.

How to reference

In order to correctly reference this scholarly work, feel free to copy and paste the following:

Yoshihiko Kuwahara and Takashi Maruyama (2010). Design of Dielectric Lens Antennas by Multi-Objective Optimization, Microwave and Millimeter Wave Technologies from Photonic Bandgap Devices to Antenna and Applications, Igor Minin (Ed.), ISBN: 978-953-7619-66-4, InTech, Available from: http://www.intechopen.com/books/microwave-and-millimeter-wave-technologies-from-photonic-bandgap-devices-to-antenna-and-applications/design-of-dielectric-lens-antennas-by-multi-objective-optimization

INTECH
open science | open minds

InTech Europe
University Campus STeP Ri
Slavka Krautzeka 83/A
51000 Rijeka, Croatia
Phone: +385 (51) 770 447
Fax: +385 (51) 686 166
www.intechopen.com

InTech China
Unit 405, Office Block, Hotel Equatorial Shanghai
No.65, Yan An Road (West), Shanghai, 200040, China
中国上海市延安西路65号上海国际贵都大饭店办公楼405单元
Phone: +86-21-62489820
Fax: +86-21-62489821

IntechOpen